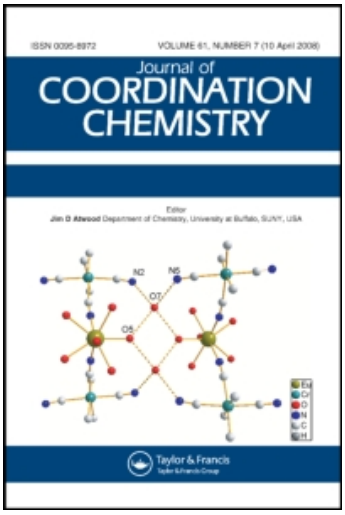

Journal of Coordination Chemistry
Publication details, including instructions for authors and subscription information:
http://www.informaworld.com/smpp/title~content=t713455674

Synthesis, characterization and XRPD studies of the bioactive complex of 2-hydroxy-3,5-dimethyl acetophenoneoxime (HDMAOX) with oxovanadium(IV)

Umesh K. Jetley[a]; Bibhesh K. Singh[b]; Bhagwan S. Garg[b]; Parashuram Mishra[b]
[a] Department of Chemistry, R. S. S. (P.G). College, Ghaziabad (NCR, Delhi), India [b] Department of Chemistry, University of Delhi, Delhi 110007, India

To cite this Article Jetley, Umesh K. , Singh, Bibhesh K. , Garg, Bhagwan S. and Mishra, Parashuram(2007) 'Synthesis, characterization and XRPD studies of the bioactive complex of 2-hydroxy-3,5-dimethyl acetophenoneoxime (HDMAOX) with oxovanadium(IV)', Journal of Coordination Chemistry, 60: 20, 2243 — 2255
To link to this Article: DOI: 10.1080/00958970701260305
URL: http://dx.doi.org/10.1080/00958970701260305

Journal of Coordination Chemistry
Vol. 60, No. 20, 15 October 2007, 2243–2255

Taylor & Francis
Taylor & Francis Group

Synthesis, characterization and XRPD studies of the bioactive complex of 2-hydroxy-3,5-dimethyl acetophenoneoxime (HDMAOX) with oxovanadium(IV)

UMESH K. JETLEY†, BIBHESH K. SINGH‡, BHAGWAN S. GARG*‡ and PARASHURAM MISHRA‡

†Department of Chemistry, R. S. S. (P.G). College, Ghaziabad (NCR, Delhi), India
‡Department of Chemistry, University of Delhi, Delhi 110007, India

(*Received 26 July 2006; in final form 23 September 2006*)

The complex of 2-hydroxy-3,5-dimethyl acetophenoneoxime (HDMAOX, HL) with VO(IV) has been synthesized and characterized by different physical techniques. Infrared spectra indicate deprotonation and coordination of the phenolic OH, and nitrogen of the oximino group. Electronic spectra and magnetic susceptibility measurements support square-pyramidal geometry around the metal ion. The elemental analyses and mass spectral data indicate ML_2 composition. Thermodynamic activation parameters were computed from the thermal data using the Coats and Redfern method. The crystal data for $C_{20}H_{24}N_2O_5V$ are: tetragonal, space group $P4/m$, $a = 11.76975$ Å, $b = 11.76975$ Å, $c = 18.89209$ Å, $V = 2617.06\,A^3$, $Z = 4$. The free ligand (HDMAOX) and its oxovanadium complex have been tested *in vitro* against *Alternaria alternate*, *Aspergillus flavues*, *Aspergillus nidulans* and *Aspergillus niger* fungi and *Streptococcus*, *Staph*, *Staphylococuss* and *Escherchia coli* bacteria in order to assess their antimicrobial potential. The results indicate that the ligand and its metal complex have antimicrobial properties.

Keywords: Spectra; Kinetics; X-ray powder diffraction; Oxovanadium complex; Bioactivity

1. Introduction

Vanadium compounds show interesting biological and pharmacological properties [1–6]. Many have insulin-mimetic activities while others possess antitumoral effects. In vertebrates, once the vanadium compounds are absorbed, they are distributed among tissues and accumulate in bones, liver and kidney [6]. Even though some simple vanadium species have beneficial biological properties, development of new vanadium derivatives with organic ligands to improve the bioavailability and decrease the toxic side effects is needed.

Acetophenoneoxime, as a bio-ligand, is important in a wide variety of applications. Different oximes and their metal complexes have shown versatile bioactivity as

*Corresponding author. Email: bibheshksingh@yahoo.co.in

Journal of Coordination Chemistry
ISSN 0095-8972 print/ISSN 1029-0389 online © 2007 Taylor & Francis
DOI: 10.1080/00958970701260305

chelating therapeutics, as drugs, as inhibitors of enzymes and as intermediates in the biosynthesis of nitrogen oxides [7]. However, with increasing use of oximes as drugs and pesticides, the intake of these chemicals followed by enzymatic oxidation may result in formation of a variety of reactive intermediates, which may lead to cell and tissue damage [8].

Acetophenone (AP, Phenylmethylketone or hypnone) is used in consumer fragrances and as an industrial solvent. Acetophenones serve as useful therapeutics against mycobacteria [9]. Some acetophenone derivatives show antimicrobial activity against gram-positive bacteria and fungi [10] while others are used as herbicides [11]. Certain acetophenones, carrying a hydroxyl group at C-2, have antimutagenic activity in *Salmonella typhimurium* [12]. Many acetophenones occur as natural products in plants [13] and fungi [14]. When orally administered to rats, paeonol (2-hydroxy-4-methoxy acetophenone) is rapidly excreted in urine as sulfated derivatives [15]. Ortho-hydroxy acetophenoneoxime also acts as an important analytical reagent for gravimetric and colorimetric estimation of transition metals [16].

We report herein the synthesis, spectral characterization (IR, electronic and mass spectra), magnetic susceptibility measurements, thermal studies and X-ray powder diffraction studies of acetophenoneoxime with VO(IV) ions. Such study may give insight into the coordination of 2-hydroxy-3,5-dimethyl acetophenoneoxime (HDMAOX) (figure 1) with VO(IV) ions. Study of the interaction of VO(IV) with oxime is of special interest from the pharmacological point of view. The bio-efficacy of the complex has also been examined against the growth of bacteria and pathogenic fungi *in vitro* to evaluate their anti-microbial potential.

2. Experiment

2.1. *Physiochemical studies*

Analyses (C, H and N) of the complex were performed using Elementar Vario EL III (Germany) model. Metal contents were estimated on an AA-640-13 Shimadzu flame atomic absorption spectrophotometer in solution prepared by decomposing the complex in hot concentrated HNO_3. An infrared spectrum was recorded on a Perkin-Elmer FT–IR spectrophotometer in KBr and polyethylene pellets. The UV-Visible spectrum was recorded in $CDCl_3$ on a Beckman DU-64 spectrophotometer while mass spectra (TOF–MS) of the complex were recorded on a Waters (USA) KC-455 model with ES^+ mode. Magnetic susceptibility measurements at room

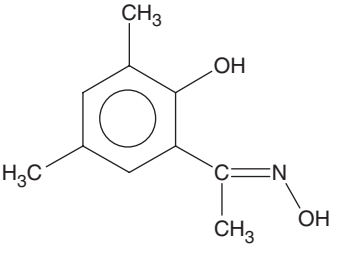

Figure 1. Structure of 2-hydroxy-3,5-dimethyl acetophenoneoxime.

temperature were carried out with powdered samples on a vibrating sample magnetometer PAR 155 with 5000G-field strength, using $Co[Hg(SCN)_4]$ as calibrant (magnetic susceptibility $\approx 1.644 \times 10^{-5}\,cm^3\,g^{-1}$). A Rigaku model 8150 thermoanalyser (Thermaflex) was used for simultaneous recording of TG-DTA curves at a heating rate of $5^\circ\,min^{-1}$. For TG, the instrument was calibrated using calcium oxalate while for DTA, calibration was done using indium metal, both of which were supplied along with the instrument in ambient conditions. A flat bed type Al-crucible was used with α-alumina (99% pure) as the reference material for DTA. The number of decomposition steps was identified using TG. The activation energy (E) and Arrhenius constant of the degradation process was obtained by the Coats and Redfern method. The XRD powder pattern was recorded on a vertical type Philips 1130/00 X-ray diffractometer, operated at 40 kV and 50 Ma generator using the Cu-Kα line at 1.54056 Å as the radiation source. The sample was scanned between 10 and 70° (2θ) at 25°C. The crystallographic data were analyzed by using the CRYSFIRE powder indexing software package and the space group was found by the GSAS program. The density was determined by Archimedes method. A metal salt was procured from Aldrich and was used as received. Solvents used were of analytical grade and were purified by standard procedures.

2.2. *Synthesis of complex*

To 50 mL of 0.2 M aqueous solution of $VOCl_2$, 100 mL of 0.4 M solution of 2-hydroxy-3,5-dimethyl acetophenone oxime (HDMAOX) [17] in 50% ethanol was added. VO(IV) formed grey coloured precipitate in the pH range 2.5–4.0. The precipitated complex was digested, filtered and washed first with hot water, then with 20% ethanol and finally dried at 105–110°C in an air oven. On the basis of elemental analysis observed (calculated) values [C: 58.98% (56.74%), H: 5.90% (5.71%), N: 6.88% (6.62%), V: 12.51% (12.03%)] in the ML_2 complex where M = VO(IV); L = 2-hydroxy-3,5-dimethyl acetophenone oxime (HDMAOX). The general composition of the complex is $[C_{20}H_{24}N_2O_5V]$. Its decomposition temperature is 180°C. Grey colored (yield 79%) crystalline complex is sufficiently soluble in chloroform for spectral measurements.

2.3. *Biological activity*

2.3.1. Antibacterial screening. *In vitro* anti-microbial (anti-bacterial) activities of the synthesized ligand and its metal complex were tested using the paper disc diffusion method [18]. The nutrient agar medium (peptone, beef extract, NaCl and agar–agar) and 5 mm diameter paper discs of Whatman No. 1 were used. The test compound was dissolved in methanol in 0.1–0.4% concentrations. The filter paper discs were soaked in different solutions of the compound, dried and then placed in the petriplates (9 mm diameter) previously seeded with the test organisms *Streptococcus*, *Staph*, *Staphylococcus* and *Escherichia coli*. The plates were incubated for 24–30 h at 27 ± 1°C and the inhibition zone (mm) was measured around each disc. As the organism grows, it forms a turbid layer, except in the region where the concentration of antibacterial agent is above the minimum inhibitory concentration, and a zone of inhibition is seen. The size of the inhibition zone depends upon the culture medium, incubation conditions, rate of diffusion and the concentration of the antibacterial agent.

2.3.2. Antifungal screening. The antifungal activity of the complexes was checked by the dry weight method for the *Alternaria alternate*, *Aspergillus flavues*, *Aspergillus nidulans* and *Aspergillus niger* fungi. The complexes were directly added to the growth medium in varying concentration (0.10–0.40% w/v). The actively growing mycelia (of the test fungi) were placed on the medium with the help of an inoculum needle and incubated at $27 \pm 1^{\circ}C$ for 7 days. The medium with the test solutions served as 'treated' while without them as 'control' or 'check'. The resulting mycelia mats in each set were carefully removed, washed, dried and then weighed separately. The fungal growth was calculated from the following relation

$$\text{Fungal growth inhibition (\%)} = 100 \times C_g - T_g/C_g$$

where C_g = average growth in the 'control' or 'check' set and T_g = average growth in the treated set.

3. Results and discussion

Elemental analysis and spectral studies reveal that the complex was of good purity. The general reaction for the preparation of the metal complex is:

$$VOCl_2 + 2HL \rightarrow [VOL_2] + 2HCl$$

3.1. *Infrared spectra and mode of bonding*

The IR spectra of the free ligand and metal complex (figure 2) were carried out in the range of 4000–400 and 400–100 cm^{-1} (table 1). The IR spectra of the ligand show a broad band between 3200 and 3450 cm^{-1}, which can be attributed to phenolic OH group. This band disappears in the complex, which can be attributed to involvement of phenolic OH in coordination. Further, the appearance of a strong band at 991 cm^{-1} in the complex may be assign to V=O stretching [19]. The shifting of broad and low intensity bands due to ν(O–H) modes of N–OH group in the 4000–3000 cm^{-1} wave number range to lower wave number at 3211 cm^{-1}suggests weakening of N–OH bond and formation of a V–N bond [7]. The medium bands observed in the 1640–1620 cm^{-1} range in the complex were assigned to ν(C=N). The shifting of the ν(C=N) vibration of the complex to lower wave number suggests that the nitrogen atom of the ring contributes to complexation. The lower ν(C=N) wave number also indicates stronger V–N binding [20, 21]. The IR spectrum of the ligand showed that ν(N–O) appears at 860 cm^{-1}. So, upon V–N interaction, ν(N–O) appears at higher wave number indicating decrease in the N–O bond length. The positive ν(N–O) shift should indicate strengthening of the V–N bond. In the IR spectrum of the complex, a band is observed between 430 and 460 cm^{-1}, attributed to the ν(V–N) stretching vibrations. Another band, between 660 and 672 cm^{-1}, is assigned to the ν(V–O) stretch [19]. A band belonging to the benzene ν(C=C) stretching vibration at 1368 cm^{-1}, appears to get affected on complexation, showing that the ligand coordinated to metal through hydroxyl oxygen on the benzene ring [22]. The band at 1374–1376 cm^{-1} in the complex is due to the $\nu(CH_3)$ and is not affected on complexation. The aliphatic protons are not greatly affected upon complexation [23].

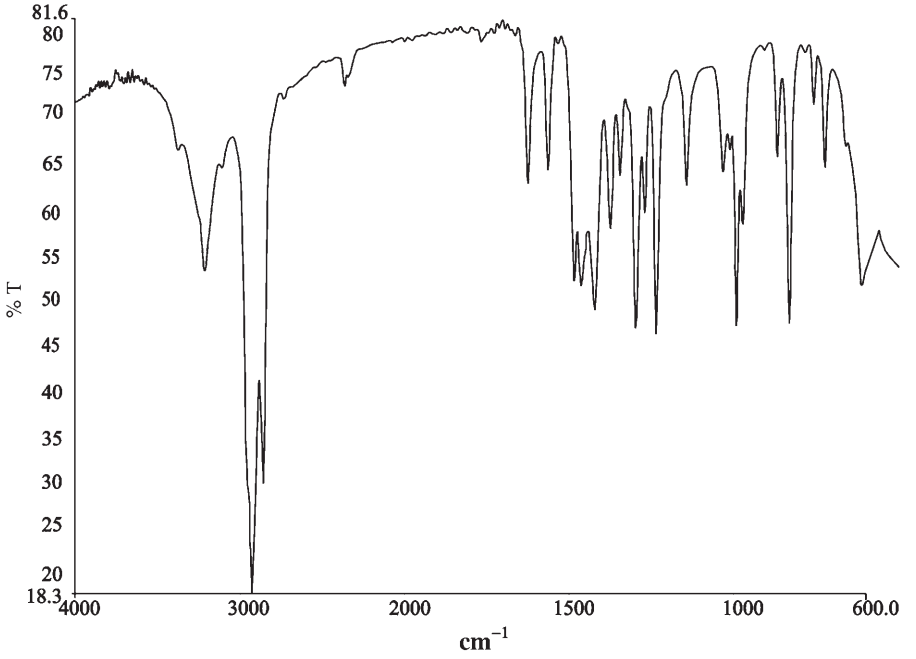

Figure 2. IR spectrum of the VO–HDMAOX complex.

3.2. *Magnetic susceptibility measurements and electronic spectra*

The magnetic moment (μ) determined at room temperature is 1.71 BM. This correlates with that of spin-only d^1 electronic configuration of the VO^{2+} cation indicating a monomeric complex [24]. The electronic spectrum of the complex (figure 3) is studied in the range 200–900 nm. Two very strong bands in the region 242–252 and 345–370 nm were observed in the spectrum of the complex, attributed to $n \rightarrow \pi^*$ and $\pi \rightarrow \pi^*$ transitions in the aromatic ring and C=N chromophore [25]. The band at 385 nm can either be assigned to the $^2B_2 \rightarrow {}^2A_1$ transition or to the low energy charge transfer/inter ligand transition. In the visible region, the spectrum of the complex shows an absorption band at 670 nm assigned to the $^2B_2 \rightarrow {}^2E$ (ν_2) in a square-pyramidal configuration [26]. It was proposed earlier that the band at 991 cm^{-1} in the infrared spectra of VO^{2+} complexes is characteristic for the aforementioned structure [19]. The present complex is a five-coordinate complex having square-pyramidal geometry with oxygen of the vanadyl group at the apex and four atoms of the ligand forming a basal plane.

3.3. *Mass spectra*

The mass spectrum of the complex (figure 4) and the characteristic molecular ion peaks has been used to confirm the proposed formula. Molecular weights (calculated) corresponding to important mass peaks for the compound are given below. The mass spectrum of complex shows many peaks corresponding to successive degradation of the molecule. It also shows a series of peaks corresponding to various fragments.

Table 1. IR spectral data (cm^{-1}), thermal data and crystallographic data of the VO(IV)–HDMAOX complex.

IR spectral data (cm^{-1})		Thermal (TG/DTA) data			Crystallographic data	
$[VO(HDMAOX)_2]$	Frequency	Parameters	Complex		Parameters	Complex
$\nu(OH)_{NOH}$	3211(m)	Order		**I**	Empirical formula	$C_{20}H_{24}N_2O_5V$
$\nu(C{=}N)$	1623(m)	Steps	**I**	**II**	Formula weight	422.91
$\delta(NOH)$	1463(s)	E^* ($J\,mol^{-1}$)	22.94	20.93	Temperature (K)	298
$\nu(CH)$	2924(s), 2855(m)	A (sec^{-1})	4.89×10^4	2.42×10^4	Wavelength (A°)	1.54056
$\nu(NO)$	972(w)	ΔS^* ($J\,K^{-1}\,mol^{-1}$)	−158.67	−168.83	Crystal system	Tetragonal
$\delta(OMO)$	190(w)	ΔH^* ($J\,mol^{-1}$)	107.17	2090.85	Space group	$P4/m$
$\delta(O–M–N)$	215(w)	ΔG^* ($kJ\,mol^{-1}$)	74.76	135.74	Unit cell dimensions (Å, °)	
					a	11.76975
					b	11.76975
					c	18.89209
					α, β, γ	90
$\nu(M–O)$	502(m)	Estimated mass loss	19.00%	60.49%	Volume (A^3)	2617.06
$\nu(M–N)$	455(m)	Calculated mass loss	19.62%	60.78%	2θ range (°)	10.00–70.00
$\nu(CH_3)$	1374(m)	Temp. range	461–478 K	752–815 K	Limiting indices	$1 \le h \le 7,\ 0 \le k \le 4,\ 0 \le l \le 9$
$\nu(C–O)$	991(s)	DTA_{max}	471 K	792 K	Density ($g\,cc^{-1}$)	1.073
s: strong	m: medium	Thermal effect	Exothermic	Exothermic	Z	4
	w: weak	Metallic residue	–	VO_2	R_f	0.0000739

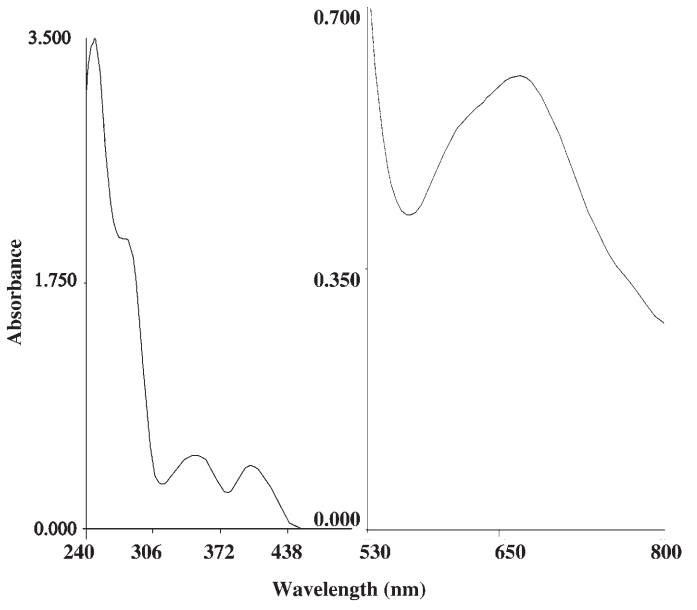

Figure 3. Electronic absorption spectrum of the VO–HDMAOX complex in $CDCl_3$.

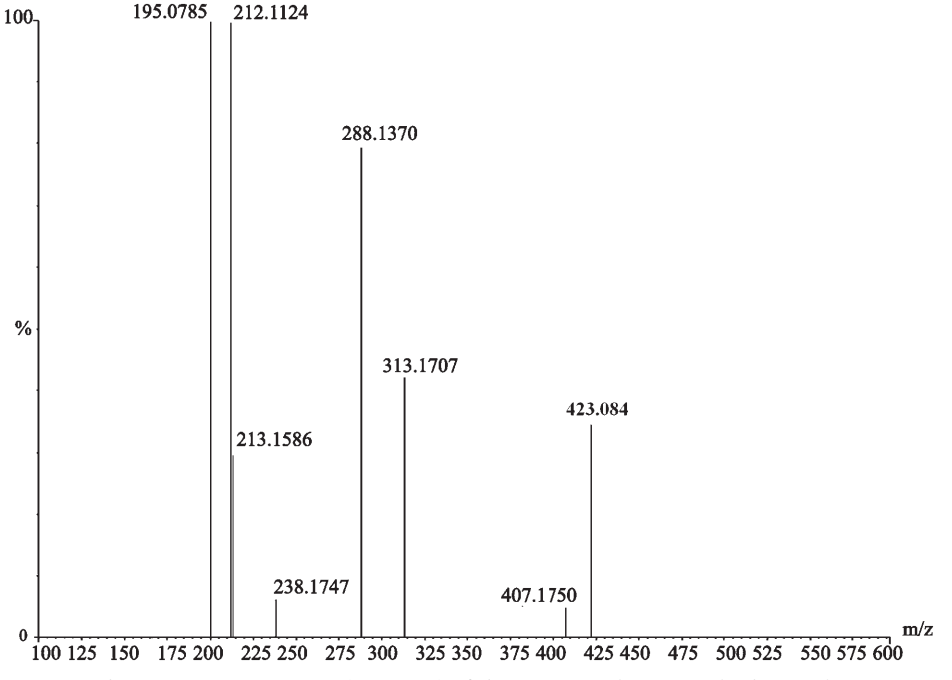

Figure 4. Mass spectrum (TOF–MS) of the VO–HDMAOX complex in $CDCl_3$.

Their intensities give an idea of stability of fragments. The two main remaining parts of the complex appear at (m/z values) of 212 and 195 (100%). These lines correspond to $[C_{16}H_{20}]^+$ and $[C_{15}H_{15}]^+$, respectively.

$$\underset{423}{[C_{20}H_{24}N_2O_5V]^+} \longrightarrow \underset{313/314}{[C_{18}H_{22}N_2O_3]^+} \longrightarrow \underset{288}{[C_{17}H_{22}NO_3]^+} \longrightarrow \underset{238}{[C_{17}H_{20}N]^+}$$

$$\downarrow$$

$$\underset{195}{[C_{15}H_{15}]^+} \longleftarrow \underset{212/214}{[C_{16}H_{20}]^+}$$

3.4. *Kinetics of thermal decomposition*

Thermogravimetric (TG) and differential thermogravimetric analyses (DTA) were carried out for VO(IV)–HDMAOX complex in ambient conditions. The thermal decomposition of $[VO(HDMAOX)_2]$ (figure 5) having the molecular formula $[C_{20}H_{24}N_2O_5V]$ proceeds with two main degradation steps. The first estimated mass loss of 19.90% (calculated mass loss = 19.62%) within the temperature range 461–478 K could be attributed to liberation of C_4H_5NO. The DTA curve gives an exothermic peak at 471 K (the maximum peak temperature). The second step occurs within the temperature range 752–815 K with an estimated mass loss 60.49% (calculated mass loss = 60.78%), which accounts for decomposition of the remainder of the ligand ($C_{16}H_{19}NO_2$) leaving VO_2 as the residue. The DTA curve gives an exothermic peak at 792 K (the maximum peak temperature). Total mass loss is 80.39% (calculated mass loss = 80.40%). The final product of decomposition at 830 K corresponds to metal oxide as the end product, confirmed by comparing observed/estimated and calculated mass of pyrolysis product.

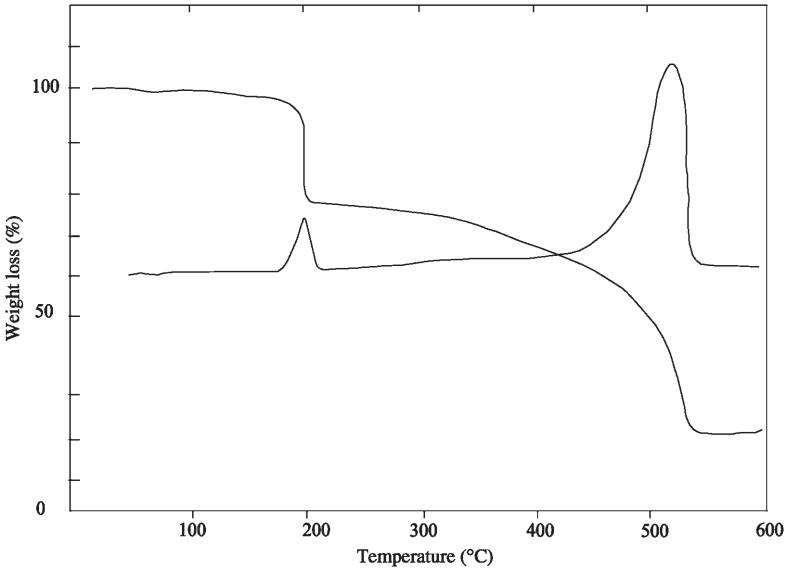

Figure 5. TG and DTA curves of the VO–HDMAOX complex.

Accordingly, the thermal decomposition mechanism can be proposed for the oxovanadium oxime complex:

$$C_{20}H_{24}N_2O_5V \xrightarrow{471\,K} C_4H_5NO + C_{16}H_{19}NO_4V$$

$$C_{16}H_{19}NO_4V \xrightarrow{830\,K} C_{16}H_{19}NO_2 + VO_2$$

The two stages of decomposition of the complex were studied in somewhat more detail. There has been interest in determining rate-dependent parameters of solid-state non-isothermal decomposition reactions by analysis of TG curves. Several equations [27–33] have been proposed to analyze a TG curve and obtain values for the various kinetic parameters. The most commonly used methods for this purpose are the differential method of Freeman and Carroll [27], the integral method of Coats and Redfern [29] and the approximation method of Horowitz and Metzger [32]. The kinetic parameters calculated by the Horowitz–Metzger method revealed no significant difference to that evaluated by the Coats–Redfern method. So, here we have used Coats–Redfern method to calculate the desired kinetic parameters.

Kinetic analysis parameters such as activation energy (ΔE^*), enthalpy of activation (ΔH^*), entropy of activation (ΔS^*), and free energy change of decomposition (ΔG^*) were evaluated graphically by employing the Coats–Redfern equation (1)

$$\log[-\log(1-\alpha)/T^2] = \log[AR/\theta E^*(1-2RT/E^*)] - E^*/2.303RT \qquad (1)$$

where α is the mass loss up to temperature T, R is the gas constant, E^* is the activation energy in J mole^{-1}, θ is the linear heating rate and the term $(1-2RT/E^*) \cong 1$. A slope of the linear plot drawn from the relevant data of the left side of equation (1) against $1/T$ gives the value of E^* while its intercept corresponds to A (Arrhenius constant). The linearization plot (figure 6) confirms the first order kinetics for the thermal change.

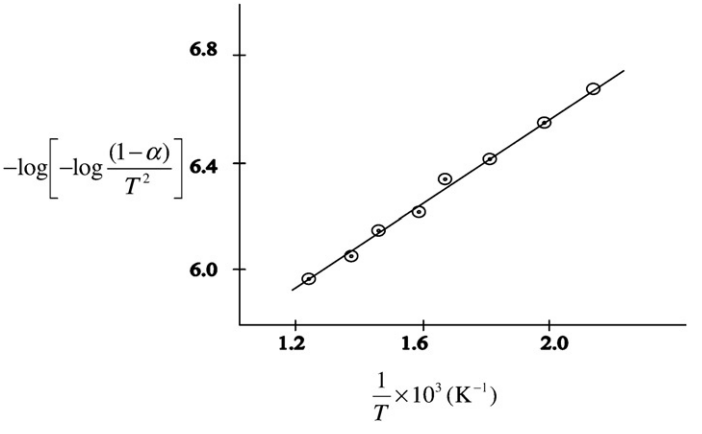

Figure 6. Kinetic linearization plot of the VO–HDMAOX complex.

The value of heat of reaction (ΔH^*) was obtained from the DTA curves by using equation (2)

$$\Delta H^* = \Delta H(\text{muv})\ 60 \cdot 10^{-6}\ \text{M J mole}^{-1} \tag{2}$$

where M is the molar mass of the complex and muv = micro unit volt. The entropy of activation (ΔS^*) and the free energy change of activation (ΔG^*) were calculated using equations (3) and (4).

$$\Delta S^* = 2.303R[\log(Ah/kT)]\ \text{J K}^{-1}\ \text{mol}^{-1} \tag{3}$$

$$\Delta G^* = \Delta H^* - T\Delta S^*\ \text{J mol}^{-1} \tag{4}$$

where k and h are the Boltzmann and Planck constants, respectively. The calculated values of E^*, A, ΔS^*, ΔH^* and ΔG^* for the decomposition steps of the complex are recorded in table 1. The complex has a negative entropy which indicates that it is formed spontaneously. The negative entropy also indicates a more ordered activated state, possibly through the chemisorption of oxygen and other decomposition products. The negative values of the entropies of activation are compensated by enthalpies of activation, leading to almost the same values for the free energies of activation [34].

3.5. *X-ray powder diffraction studies*

X-ray powder data are useful to deduce accurate cell parameters. The indexing procedures were performed using the (CCP_4, UK) Crysfire programme [35] giving tetragonal crystal system for [VO(HDMAOX)$_2$] (figure 7) having M(8) = 6, F(8) = 2, as the best solutions. Their cell parameters are shown in table 1.

3.6. *Antimicrobial activities*

The free ligand and its oxovanadium complex were screened against *A. alternate*, *A. flavus A. nidulans* and *A. niger* fungi and *Streptococcus*, *Staph*, *Staphylococuss* and *E. coli* bacteria to assess their antimicrobial activity. It is clear from the antifungal screening data (figure 8a and b) that the metal complex is more fungitoxic than the chelating agent itself. The oxovanadium complex showed maximum activity against *A. alternate* fungi. The bacterial screening results (figure 8c and d) reveal that the free ligand (HDMAOX) showed maximum activity against *Streptococcus* bacteria whereas its oxovanadium complex showed the maximum activity against *Staphylococuss* bacteria and activity was the least against *Staph* bacteria. The antibacterial data reveal that the complex is superior to the free ligand. The enhanced activity of the metal complex may be ascribed to the increased lipophilic nature of the complex arising due to chelation [36]. It was also noted that the toxicity of the metal chelate increases on increasing concentration.

It can be concluded from above results that oxovanadium–HDMAOX complex is five coordinated with square-pyramidal geometry with oxygen of the vanadyl group

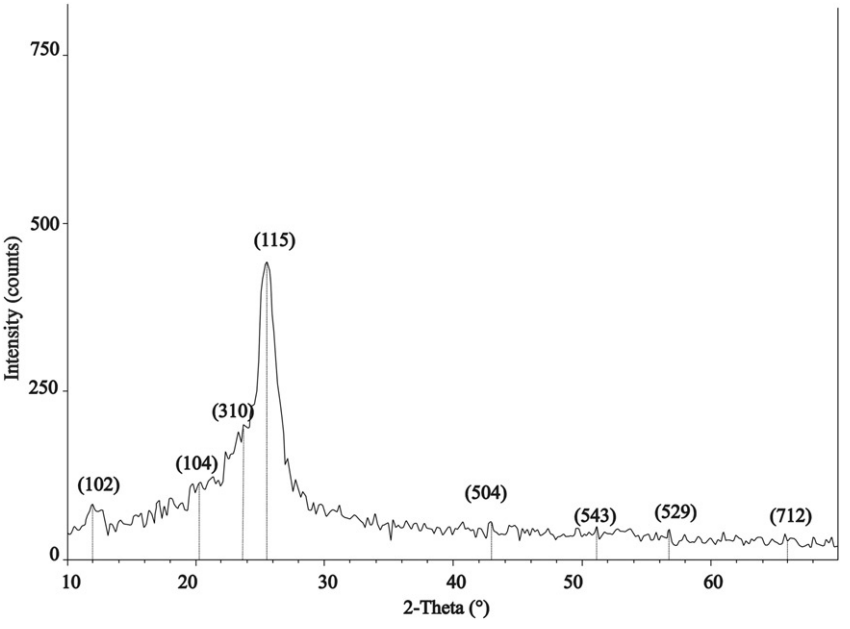

Figure 7. XRPD plot of the VO–HDMAOX complex.

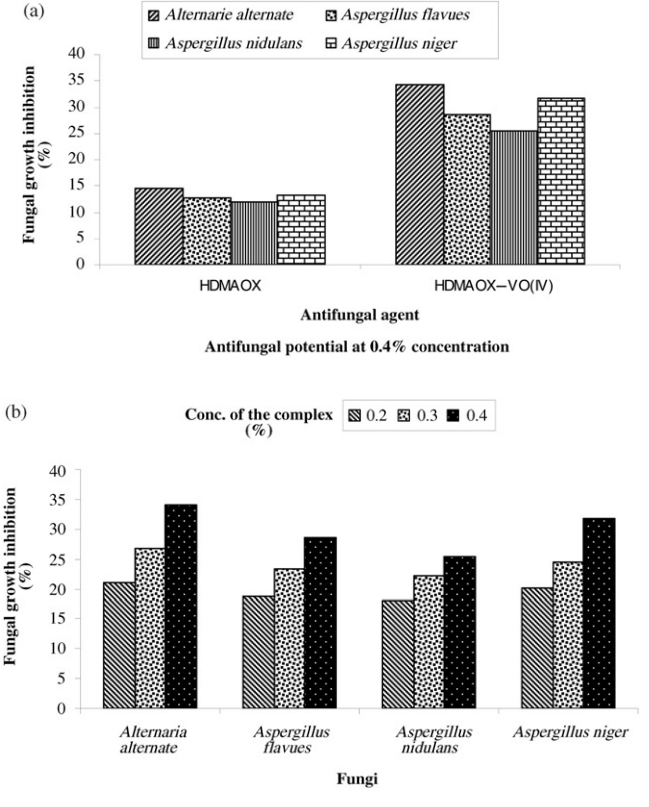

Figure 8. Antifungal screening.

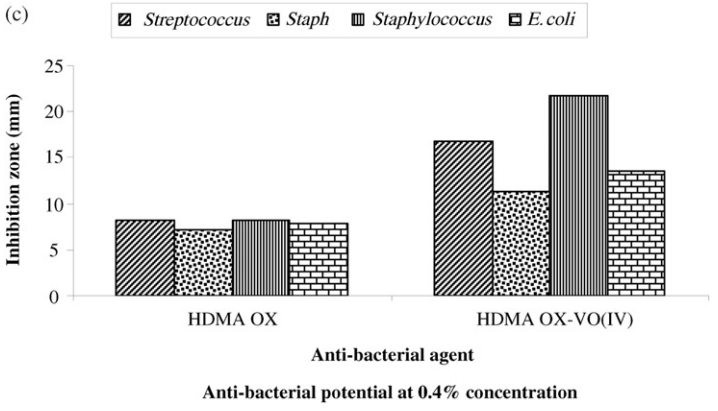

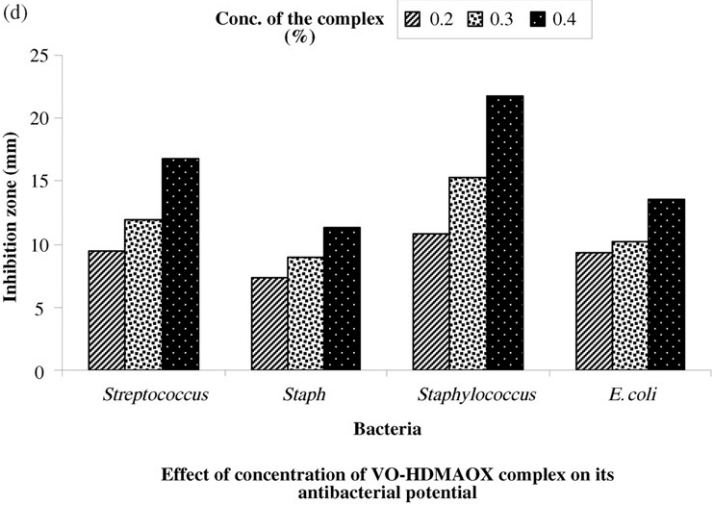

Figure 8. Continued.

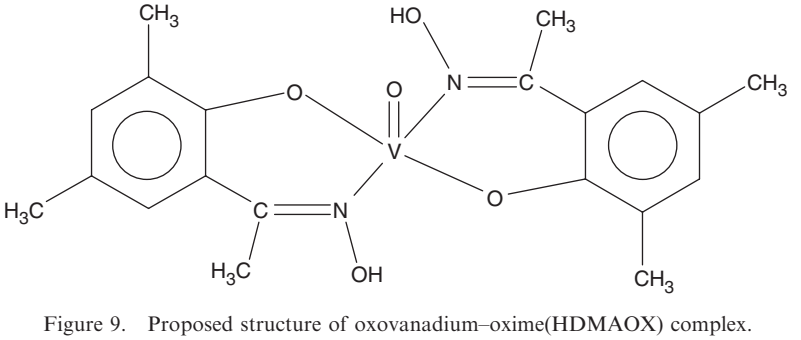

Figure 9. Proposed structure of oxovanadium–oxime(HDMAOX) complex.

at the apex and four atoms of the ligand placed in the basal plane. The proposed structure of the complex is as shown in figure 9.

Acknowledgement

One of the authors (B.K. Singh) is thankful to University Grants Commission, New Delhi, India for financial assistance under the research award scheme. The author UKJ is thankful to the Principal, R. S. S. (P.G) College, Ghaziabad (NCR, Delhi), India for providing necessary lab facilities.

References

[1] E.J. Baran, J. Braz. *Chem. Soc*., **14**, 878 (2003).
[2] D. Rehder. *Inorg. Chem. Commun*., **6**, 604 (2003).
[3] K.H. Thompson, C. Orvig. *Coord. Chem. Rev*., **219/221**, 1033 (2001).
[4] A. Morinville, D. Maysinger, A. Shaver. *Trends Pharmacol. Sci*., **19**, 452 (1998).
[5] S.B. Etcheverry, D.A. Barrio, J. Zinczuk, P.A.M. Williams, E.J. Baran. *J. Inorg. Biochem*., **99**, 2322 (2005).
[6] B. Mukherjee, B. Patra, S. Mahapatra, P. Banerjee, A. Tiwari, M. Chatterjee. *Toxicol. Lett*., **150**, 135 (2004).
[7] I. Georgieva, N. Tredafilova, G. Bauer. *Spectrochim. Acta A*, **63**, 403 (2006).
[8] A. Park, N.M. Kosareff, J.S. Kim, H.J. Peter de Lijser. *Photochem. Photobiol*., **82**, 110 (2006).
[9] L. Rajabi, C. Courreges, J. Montoya, R.J. Aguilera, T.P. Primm. *Lett. Appl. Microbiol*., **40**, 212 (2005).
[10] H.I. Gul, A.A. Denizci, E. Erciyas. *Arzneimittel – Forsch*., **52**, 773 (2002).
[11] M. Teruyuki, H. Yoshiharu, Y. Ka. Oxime derivative thereof, Process for preparing thereof, Herbicidal composition and methods for the destruction of undesirable weeds. Japan; Asahi Chemical Ind. (1986).
[12] M. Miyazawa, H. Shimamura, S. Nakamura, W. Sugiura. *J. Agr. Food Chem*., **48**, 4377 (2000).
[13] C. Guyot, A. Bouseta, V. Scheirman, S. Collin. *J. Agr. Food Chem*., **46**, 625 (1998).
[14] C.K. Wilkins, S. Scholl. *Int. J. Food Microbiol*., **8**, 11 (1989).
[15] T. Yasuda, R. Kon, T. Nakazawa, K. Ohsawa. *J. Nat. Prod*., **62**, 1142 (1999).
[16] S.N. Poddar. *Anal. Bioanal. Chem*., **154**, 254 (1957).
[17] W. Nogami. *J. Pharm. Soc. Jpn*, **61**, 46 (1941).
[18] C. Saxena, D.K. Sharma, R.V. Singh. *Phosphorus, Sulfur*, **85**, 9 (1993).
[19] N. Raman, A. Kulandaisamy, C. Thangaraja, K. Jeyasubramanian. *Transit. Met. Chem*., **28**, 29 (2003).
[20] K. Nakamoto. *Infrared and Raman Spectra of Inorganic and Coordination Compounds*, Wiley, New York (1978).
[21] R.M. Silverstein, G.C. Basler, T.C. Morril. *Spectrometric Identification of Organic Compounds*, Wiley, NewYork (1974).
[22] W. Li, Q. Wu, Y. Ye, M. Luo, L. Hu, Y. Gu, F. Niu, J. Hu. *Spectrochim. Acta A*, **60**, 2343 (2004).
[23] N.M. Shauib, Abdel-Zaher A. Elassar, A. El-Dissouky. *Spectrochim. Acta A*, **63**, 714 (2006).
[24] A. Syamal. *Coord. Chem. Rev*., **16**, 309 (1975).
[25] D.H. Williams, I. Fleming. *Spectroscopic Methods in Organic Chemistry*, 4th Edn, McGraw Hill, London (1989).
[26] N.M. El-Metwally, R.M. El-Shazly, I.M. Gabr, A.A. El-Asmy. *Spectrochim. Acta A*, **61**, 1113 (2005).
[27] E.S. Freeman, B. Carroll. *J. Phys. Chem*., **62**, 394 (1958).
[28] J. Sestak, V. Satava, W.W. Wendlandt. *Thermochim. Acta*, **7**, 333 (1973).
[29] A.W. Coats, J.P. Redfern. *Nature*, **68**, 201 (1964).
[30] T. Ozawa. *Bull. Chem. Soc. Jpn*, **38**, 1881 (1965).
[31] W.W. Wendlandt. *Thermal Methods of Analysis*, Wiley, New York (1974).
[32] H.H. Horowitzt, G. Metzger. *Anal. Chem*., **35**, 1464 (1963).
[33] J.H. Flynn, L.A. Wall. *Polym. Lett*., **4**, 323 (1966).
[34] B.K. Singh, R.K. Sharma, B.S. Garg. *J. Therm. Anal. Calorim*., **84**, 593 (2006).
[35] R. Shirley. The CRYSFIRE system for automatic powder indexing: Users manual (Lattice Press) (2002).
[36] L.D.S. Yadav, S. Singh. *Indian J. Chem*., **40B**, 440 (2001).